A Driver State Detection System—Combining a Capacitive Hand Detection Sensor With Physiological Sensors

Stephan Mühlbacher-Karrer, Ahmad Haj Mosa, Lisa-Marie Faller, Mouhannad Ali, Raiyan Hamid, Hubert Zangl, and Kyandoghere Kyamakya

***Abstract*— With respect to automotive safety, the driver plays a crucial role. Stress level, tiredness, and distraction of the driver are therefore of high interest. In this paper, a driver state detection system based on cellular neural networks (CNNs) to monitor the driver's stress level is presented. We propose to include a capacitive-based wireless hand detection (position and touch) sensor for a steering wheel utilizing ink-jet printed sensor mats as an input sensor in order to improve the performance. A driving simulator platform providing a realistic virtual traffic environment is utilized to conduct a study with 22 participants for the evaluation of the proposed system. Each participant is driving in two different scenarios, each representing one of the two no-stress/stress driver states. A "threefold" cross validation is applied to evaluate our concept. The subject dependence is considered carefully by separating the training and testing data. Furthermore, the CNN approach is benchmarked against other state-of-the-art machine learning techniques. The results show a significant improvement combining sensor inputs from different driver inherent domains, giving a total related detection accuracy of 92%. Besides that, this paper shows that in case of including the capacitive hand detection sensor, the accuracy increases by 10%. These findings indicate that adding a subject-independent sensor, such as the proposed capacitive hand detection sensor, can significantly improve the detection performance.**

***Index Terms*— Artificial neural networks, automotive applications, capacitive sensors, cellular neural networks (CNNs), ink-jet printing.**

I. Introduction

A. Motivation

THE detection and the monitoring of a driver state play an important role in automotive safety. The driver's inattention is a major cause of traffic accidents as reported in [1]. Also, in highly automated driving (e.g., traffic jam assistant/automation [2]), the driver still plays an important role when it gets to the point, where the vehicle relinquishes control.Besides this, the Vienna Convention on Road Traffic states that the driver must be able to take back control of the vehicle at any time and as long as the driver is involved in operating the vehicle, the driver has a major influence on its safe operation.

In [3], the proposed driver state system gets its input data from different domains, i.e., driver inherent (biometrics, emotion, driving behavior, and visual attention) and external demands (environmental conditions). The biometric sensors obtain the data of the physical condition of the driver, e.g., the heart rate, ElectroEncephaloGraphy (EEG), blood pressure, and so on. The driving behavior domain, for instance, contains the speed, following distance, and so on. In this sense, not only monitoring whenever the hand touches the steering wheel, but also to monitor its position on the steering wheel while driving might be important as additional input to characterize the driver state in many cases including, e.g., psychological studies.

Therefore, a sensor is needed, which fulfills the following requirements:

1) simultanous touch and position sensing;
2) capability to be integrated into an electrical control unit (ECU);
3) rapidly and efficiently adaptable;
4) easy retrofit to be suitable for in-car use and driving simulator platforms [4].

To evaluate the usability of the proposed sensor, a suitable driver state detection system is necessary, which is able to incorporate and process all input data from different domains, i.e., biometrics and driving behavior domain. The driver state detection is a machine learning task that can be realized through one of the common pattern recognition techniques, such as support vector machine (SVM) [5], [6], Bayesian method [7], [8], or Artificial neural network (ANN) [9], [10]. ANNs have shown several useful features that include the following:

1) ability of modeling both, linear and nonlinear data;
2) nonparametric, i.e., ANNs do not need an explicit underlying model;
3) can be used for complex data structures/models due to their flexibility and universality [11].

The flexibility of ANNs motivated the researchers to develop various architectures such as nonlinear autoregressive network, long short-term memory (LSTM), or cellular neural

Manuscript received June 10, 2016; revised September 5, 2016; accepted October 21, 2016. This work was supported in part by the DEWI Project through the ARTEMIS Joint Undertaking under Grant 621353 and in part by the Austrian Research Promotion Agency (FFG) under Grant 842547. The Associate Editor coordinating the review process was Dr. Salvatore Baglio.

S. Mühlbacher-Karrer, L.-M. Faller, R. Hamid, and H. Zangl are with the Sensors and Actuators, Institute of Smart System Technologies, Alpen-Adria-Universität Klagenfurt, 9020 Klagenfurt, Austria (e-mail: stephan.muehlbacher-karrer@aau.at).

A. H. Mosa, M. Ali, and K. Kyamakya are with the Institute of Smart System Technologies, Transportation Informatics, Alpen-Adria-Universität Klagenfurt, 9020 Klagenfurt, Austria.

Color versions of one or more of the figures in this paper are available online at http://ieeexplore.ieee.org.

Digital Object Identifier 10.1109/TIM.2016.2640458

networks (CNNs). CNN is a continuous recurrent neural network (RNN) that has been utilized successfully in various classification cases [12]–[14]. However, a more powerful CNN requires a high number of cells/neurons, which leads to a higher training complexity when using CNN traditional learning methods [15]–[17]. Recently, the echo state network (ESN) has emerged as a promising learning technique for RNN [18]. In this paper, we use the ESN paradigm to train the proposed CNN. In the following, we summarize the advantages of a CNN.

1) The task of emotion recognition is done using a highly nonlinear dynamical system, in which the history of inputs has impact on the output. This implies that the utilized model should have a memory that considers the history of its inputs. As Jaeger presented in [19], RNNs involving ESN insure a LSTM feature, when a large number of neurons are used and/or modeled as a continuous RNN.
2) Due to its huge parallelism capability, CNN is a real-time processor that can be realized/implemented either in hardware and thereby either in dedicated analog circuits [20], [21] or in software. It can also be emulated on top of digital platforms, such as Field Programmable Gate Array (FPGA). and GPU [22], [23].
3) CNN applications in classification show a remarkable performance according to published related work [13], [14], [24].

B. Related Work

Capacitive sensing is widely used in the automotive industry [25] for the detection of humans, e.g., seat occupancy [26] or smart car trunk opener [27]. Common human hands ON/OFF detection sensor systems [28] utilize sensors integrated in the steering wheel rim. Such devices exploit various sensing technologies, such as capacitive, resistive and others. Patents for hand position sensing devices including a feedback device [29] and patents for hands ON/OFF detection including an emergency response system [30] exist. The proposed capacitive hand detection sensor (CHDS) combines both position and touch detection simultaneously.

Energy management plays a major role in wireless sensor networks (WSNs). Since sensor nodes are limited in size, their energy sources are limited in many applications. Frequent replacement of batteries due to energy drain can impair the benefit of wireless sensing. Usually, the wireless data communication module consumes the majority of the power supplied to the system. Data compression is therefore implemented as a mean to reduce energy consumption. Reference [31] outlines how a swinging door compression algorithm can be employed as a mean to reduce the amount of data necessary to be transmitted, and therefore, it improves the energy performances of nodes in WSN.

Processes of the category of additive manufacturing, such as 3-D and ink-jet printing, promise easy integration in existing production lines due to their versatility. They enable manufacturing of different designs on the same production line with little down time [32]. Ink-jet printing provides great potential for electronics manufacturing and rapid prototyping in general as well as sensor construction (e.g., [33], [34], or [35]) and fabrication of antennas and RFID tags [36], [37]. It further enables manufacturing of application specific sensor front ends at comparably low costs. Additionally, the suitability of printed sensors for usage in automotive applications has been demonstrated [38].

The detection of a driver state is a critical task that has been studied by several researchers. In [39], it is demonstrated that physiological sensors can be used successfully in a driver state detection. They have carried out a study with 24 drivers who were asked to drive in three different driving scenarios, which represent three stress levels (low, medium, and high). The obtained detection accuracy is equal to 97%, the evaluation is done by utilizing the "leave one out" cross validation technique. A technique that is subject-dependent, since, at least two states of the tested driver are used in the training process. A discussion of the difference between subject dependence and subject independence is provided in [40]. The conclusion was that the subject-dependent (train and test on the same driver) emotion detection performance (95%) is much higher than the subject-independent (train and test on different drivers) emotion detection (70%), which is discussed in this paper.

In [41], a detection system for a driver's emotions (engagement, enjoyment, frustration, and boredom) is presented. The drivers were asked to use a driving simulator platform while accomplishing a variety of driving assignments, e.g., following the route of a navigation system while not violating any traffic rules. The emotion is assessed then by a therapist who is monitoring the driver's behavior. A "tenfold" cross validation method is used, which considers subject independence. Different classification methods (SVM, BayesNet, multilayer perceptron, decision tree, and random forest) are evaluated. The highest presented accuracy of the four emotions: engagement, enjoyment, frustration, and boredom is 77.78%, 79.63%, 79.63%, and 81.48%, respectively.

In [42], a hybrid driver distraction detection system utilizing subject-independent sensors in combination with SVM is introduced, where an average detection accuracy of 81.1% is obtained. Recent investigations [43] show an improvement of the accuracy to 88% and 90% for Bayesian network and SVM approaches for the detection of the cognitive driver distraction. In [44], it was found that cognitive distraction has an impact on the steering behavior of the driver, leading to a decrease of the steering smoothness. The benefit of combining subject-dependent and subject-independent sensors is investigated in [45] and shows an improvement of the accuracy. A review of driver inattention monitoring systems can be found in [46].

Generally, the main drawback of the earlier methods considering only physical sensors is the low accuracy due to their subject dependence. Consequently, the CHDS is suggested to be combined with a promising neurocomputing model to reduce the subject dependence problem.

C. Contribution

To evaluate the CHDS, we present a driver state detection system based on CNN to monitor the stress level of the driver.

Fig. 1. Driving simulator platform used for the experiments with the capacitive sensor equipped steering wheel [4].

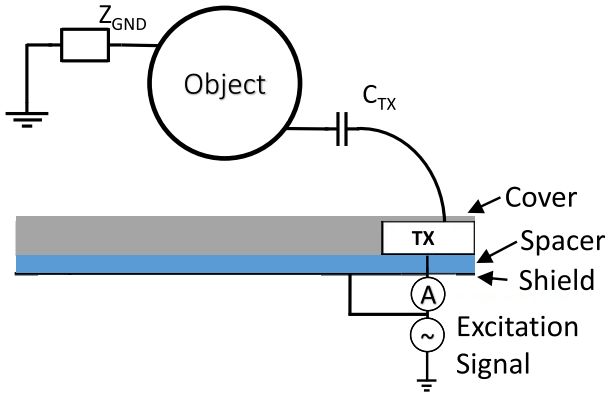

Fig. 2. Single-ended measurement mode of a CDC comprising the transmitter (TX) electrode, a spacer, and a shield layer at the bottom [48].

The system takes the data of physiological sensors and the proposed wireless CHDS for a steering wheel and extracts additional input data in comparison to other driver detection systems [39], in order to reduce the subject dependence. The front end of the capacitive sensor is realized using ink-jet-printed electrodes on a bendable substrate. These sensor mats are more flexible than the state-of-the-art flex prints and are used to detect, where the hand of the driver touches the steering wheel. Due to the implemented energy management, wireless data transmission, and different available power supplies (USB and battery), the CHDS is ready to be integrated into a steering wheel. In addition, the proposed CHDS enables also retrofitting of any car to run a study in real traffic environment. In this setup, the sensor is fully integrated on an original equipment manufacturer steering wheel for the driving simulator platform shown in Fig. 1. The driving simulator platform provides a realistic virtual test scenario to conduct a study to detect the driver state and validate the proposed concept.

The remainder of this paper is structured as follows. In Section II, we describe the proposed sensor system, and in Section III, the driver state detection concept is presented. The experimental setup, the study, and the obtained results are described in detail in Section IV. Finally, the conclusion is given in Section V.

II. Sensor System Description

A. Capacitive Sensor

The measurement principle is based on the interaction of a human with an electric field while approaching/touching the sensor front end (electrodes). In this paper, a capacitance-to-digital converter (CDC) operating in single-ended measurement mode [47], where the capacitance between a transmitter and the distant ground is measured is used, as shown in Fig. 2.

An excitation signal with $f_{\text{exc}} = 250$ kHz and an amplitude of $V_{\text{exc}} = 3.3$ V is applied on the transmitter electrode. The human hand approaching the electrode distorts the electric field. The resulting change of the capacitance between the transmitter electrode and the distant ground is measured. We want to detect the position as well as how intense a hand/finger of a driver touches/grasps the steering wheel. These actions can result in a capacitance change as small as several femtofarads according to our simulations (see Section II-A1). Consequently, we decided to use a 16-b high resolution (in the range of femtofarad) sigma-delta CDC providing a good tradeoff between resolution, conversation speed, and power consumption (it should be noted that the raw measurement data of the CDC are used as input features of the CNN, see Section II-A4). Furthermore, the CDC should be fully qualified for automotive applications and capable to be integrated into an ECU.

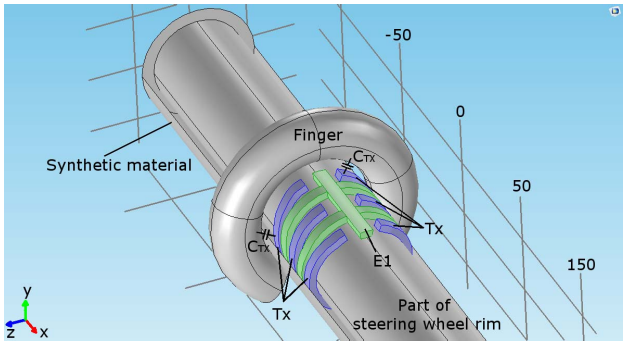

Fig. 3. Geometry model of the finite-element method simulation of the electrode structure configured for the single-ended measurement mode. The geometry model comprises the transmitter electrode Tx (blue) wrapped around the steering wheel rim approximated by a cylinder and a finger. The electrode in the middle E1 (green) is only used in the setup of [4].

1) Simulations: A simulation model is setup to determine a feasible electrode structure usable for both single-ended and differential measurement mode [4], which is mountable on the steering wheel (see Fig. 5). A snapshot of the used geometry for the simulation is shown in Fig. 3. The finger is approximated as a torus with diameter $d = 1.4$ cm that is well coupled to ground (same as a human) and the electrodes are wrapped around a cylinder with the same diameter as the steering wheel rim. In this illustration, the single-ended measurement mode becomes clear, where the capacitance C_{TX} between the transmitter electrode (Tx) and distant ground is determined. In comparison with [4], the electrodes that are not used in the single-ended measurement setup are set to active guard (see Fig. 3).

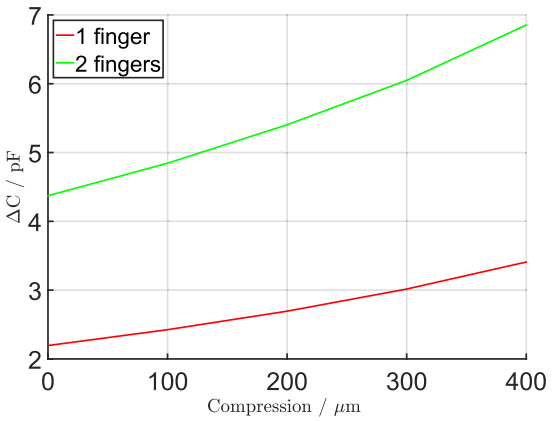

Fig. 4. FEM simulation results of the geometry model, where one and two fingers touch and compressing the synthetic material up to 400 μm.

In Fig. 4, the simulation results for one and two fingers touching the surface of the covered electrodes, compressing the synthetic material up to 0.4 mm, are shown. The resolution of the CDC is chosen according to the obtained average change of capacitance per micrometer compression for one finger of the simulation results, which is $\approx$3 (fF/μm).

2) Sensor Node: The sensor node is based on an ultralow power wireless system on a chip from Nordic Semiconductors (nRF51822 [49]) suited for wireless applications. It is composed of a 16-b CDC AD7147 [50] with 13 inputs. The chosen CDC has a current consumption of 1 mA [or 77 (μA/channel)] in the full power mode and 21.5 μA [or 1.65 (μA/channel)] in the low power mode, with an update rate of at least 107 Hz for all 13 input channels. Furthermore, the CDC fulfills all requirements for automotive applications. The single-ended measurement CDC was chosen, because the results in Section IV show a more robust performance than the results presented in [4]. Comparing the single-ended measurement with the differential measurement CDC, the maximum obtained signal amplitude is eight times higher while grasping the steering wheel. Furthermore, no shielding effect occurs in the single-ended measurement mode and the dynamic range increases up to DR $= 20\log((C_{\max})/(C_{\text{noise}})) = 19$ dB. The sensor node can be powered via USB, battery, or the steering wheel's power supply. The sensor node electronics fulfill the space requirements to place it inside the chassis of the steering wheel. Up to two sensor mats consisting of six electrodes can be connected to the sensor node and can be attached on the left and right sides of the steering wheel to monitor a driver's hand position [4].

3) Sensor Mat: The electrodes of a sensor mat have an interdigital design as obtained from the simulations with a finger length of $d_l = 70$ mm and a spacing of up to $d_s = 4$ mm between each finger. The electrode structure is shown exemplary in Fig. 5.

Each sensor mat has a four layer structure, where the electrodes are sandwiched by isolation layers and placed on top of the bottom shielding layer. Manufacturing the electrode layer utilizing ink-jet printing results in a height of a printed conductive layer of approximately $d_e = 200$ nm. Due to the design process, the sensor mat is highly bendable and can

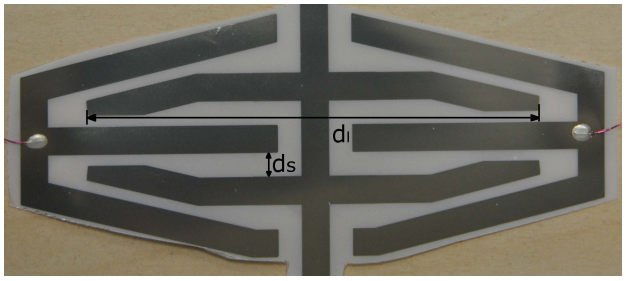

Fig. 5. Structure for one out of six inter digital electrodes of a sensor mat, e.g., the transmitter (Tx1) covering an area (A1) of the steering wheel rim [4].

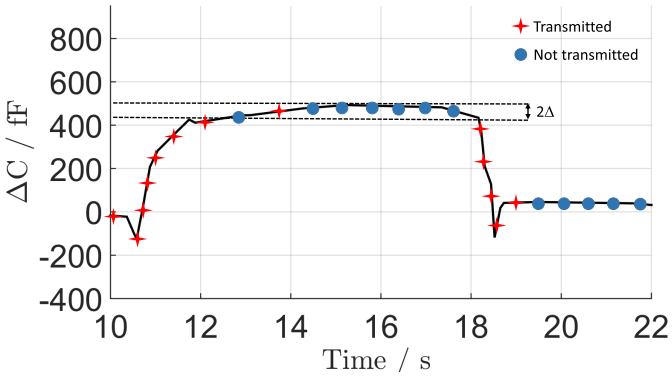

Fig. 6. Illustration of the compression approach, where the signal is not transmitted as long as the signal change is not greater than 2Δ [4].

be easily wrapped around the steering wheel rim. It can be mounted underneath or on top of the steering wheel rim cover. The sensor mats can be used either with the sensor node with the differential measurement CDC of [4] or with the single-ended measurement CDC as presented in this paper.

4) Energy Efficient Data Transmission: In [51], it was proposed to use an energy efficient data transmission technique for transmitter and receiver side (see Fig. 6), which omits the transmission of redundant data leading to a reduced amount of data to be transmitted, while at the same time, no information is lost at the receiver side. The technique is implemented on the transmitting sensor node to minimize its power consumption, which is an important factor for automotive applications. The minimum valid transmission rate for the sensor is the heartbeat rate. This rate is maintained even if the change of the signal is smaller than 2Δ. In this paper, the heartbeat rate of the sensor is set to $t_{hb} = 2$ s. This leads to a measured average power consumption for the data transmission of the sensor node of $P_{hb} = 2.85$ mW, while only heartbeat signals are transmitted. In comparison, in continuous transmission, the measured average power consumption for data transmission increases to $P_{\text{avg}} = 5.79$ mW. Depending on the measured signal, the power consumption for the data transmission of the sensor node can be reduced up to 49.3% without loss of any information on the receiver side in the full power mode [4].

The sensor node is placed in the center of the steering wheel, transmitting the data via a 2.4-GHz radio link to a receiver dongle connected to a PC providing full flexibility [4].

5) Calibration and Detection: An offset calibration is done since we are only interested in the signal change, while a human hand is grasping the steering wheel. In this respect, the

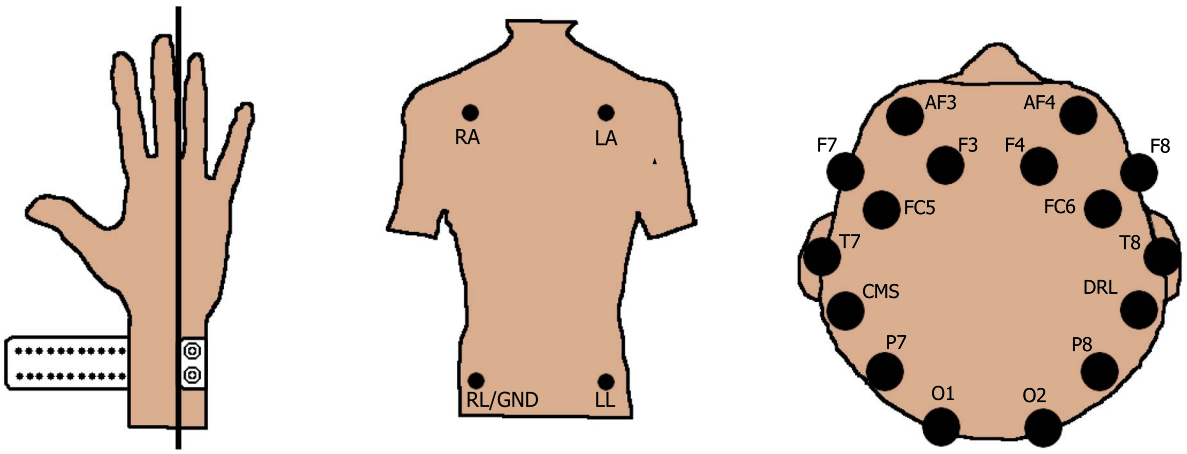

(a) (b) (c)

Fig. 7. Position of different physiological sensors on a human body. (a) Placement of EDA sensors [52]. (b) Position of the four ECG electrodes [53]. (c) Placement of 14 EEG channels and 2 references channels [54].

mean value of the raw sensor signal C_{raw} (human hand is not touching the steering wheel nor approaching it) is subtracted from the current measurement signal C_{cur} at each time

$$\Delta C = C_{\text{raw}} - C_{\text{cur}}. \tag{1}$$

A raise of a sensor signal above a predefined threshold value ΔC_{th} triggers the detection of a human hand in a dedicated area [A1–A12, see Fig. 12(b)] grasping the steering wheel rim [4].

B. Physiological Sensors

We consider the following physiological sensors for the driver state estimation study. It should be noted that no cameras are used, e.g., for face recognition, due to privacy protection of the participating subjects of the study.

1) ElectroDermal Activity: The electrodermal activity (EDA) sensor measures skin's ability to conduct electricity, which increases if the skin is sweaty. The EDA signals are measured with a sampling rate of $f_{\text{sEDA}} = 4$ Hz using a wearable wireless device (Empatica-E4 [52]). Fig. 7(a) shows the placement of the EDA sensor on the human wrist.

2) ElectroCardioGram: The electrocardiogram (ECG) sensor measures the electrical activity of the heart over a period of time using electrodes placed on a human body. The wearable wireless Bioradio device [53] is used to measure the ECG signal with three electrodes (plus one ground electrode) placed on the body [see Fig. 7(a)] at a sampling rate of $f_{\text{sECG}} = 500$ Hz.

3) EEG: The EEG sensor measures the brain waves using electrodes attached to the scalp. A wireless 14 channel (electrodes) EEG measurement device Emotiv Epoc [54] is used with a sampling rate of $f_{\text{sEEG}} = 128$ Hz to obtain the EEG signals. The location of the 14 electrodes on the head is based on the International 10- 20 system [55] [see Fig. 7(c)].

To further reduce the complexity and increase the usability of the system for the driver, in [56], physiological sensors, e.g., to measure the heart rate, are presented, which are integrated in the driver seat.

III. Driver State Estimation Concept

The estimation of the driver state is done using a neurocomputing framework that uses a CNN as core concept. In order to realize the framework, two aspects need to be considered. First, the state of a driver does not change immediately, and it is rather subject to a transient phase between the states. Thus, the system needs to observe the history of the sensor measurements before making a decision about the driver state [41]. The second aspect is the expected complexity of the system training. This complexity is caused by the amount of high-dimensional sensor data. Sections III-A–III-F present our CNN framework, including the raw data preprocessing, features extractions, and the learning process of the framework.

A. Feature Extraction

From each of the physiological signals, we have extracted 12 EDA features, 8 ECG features (per-channel), 25 EEG features (per-channel), and 12 CHDS raw features, respectively, with the time windows of $t_w = 10$ s length, from various analysis domains including time and frequency.

1) EDA Features: The EDA signal consists of the skin conductance level (SCL) as slow changing part and the skin conductance responses (SCRs) as phase components, which are the short-term conductance changes. Conventional statistics obtained from the SCL analysis have been found to be well correlated with emotion [57]. Different statistic measurements are calculated, including the following: the mean, the standard deviation, the maximum, the minimum, the root mean square, the mean of the first derivation, the mean of the second derivation, and the mean of the negative slope. Moving to the SCR analysis, we calculate the rate of SCR occurrences from the very low frequency band (0–0.1 Hz), the response latency of the first significant SCR, the sum of SCR amplitudes, and the sum of SCR areas [57].

2) ECG Features: The ECG features are separated into two different types. First, the statistical time-domain features

include the following: the mean and the standard deviation of the beat-to-beat interval (NN interval), the root mean square of differences of successive NN intervals, the number of successive differences that are greater than 50 ms, and the percentage of total intervals that successively differ by more than 50 ms, which is a standard threshold. Second, the frequency domain features, we extract the average power of the low frequency range (0.04–0.15 Hz) and the high frequency band (0.15–0.4 Hz), as well as the ratio of power within the low frequency band to that within the high frequency band [58].

3) EEG Features: Discrete wavelet transform is used to analyze the EEG signals. We have selected Daubechies wavelet because of its smoothing features, which gives the ability of detecting the EEG changes [59]. The number of the wavelet's decomposition levels are determined depending on the dominant frequency components of the signals [60]. Here, the sampling rate of EEG signals is $f_{\text{sEEG}} = 128$ Hz. Therefore, five levels Daubechies wavelet of order 4 (db4) are used to extract the subbands of brain waves delta (0.1–4 Hz), theta (4–8 Hz), alpha (8–13 Hz), beta (13–30 Hz), and gamma (30–64 Hz) [61]. Moreover, from these subbands, we extract the following features: the mean, the standard deviation, the root mean squared logarithmic, the wavelet energy, and the wavelet entropy [62], [63]. In general, 25 features are extracted from each EEG channel.

4) CHDS Features: In the case of CHDS, we do not extract any extra features. The measurement raw data are used as raw features. This is done to additionally detect if the driver is slightly touching or sliding his hand on the steering wheel. The average sampling rate of CHDS is $f_{\text{sCHDS}} = 20$ Hz.

B. Data Synchronization

The physiological and CHDS signals have different sampling rates. For that, all signals have to be synchronized using a reference timestamp. In this paper, we are using the starting time of the EEG signals as a start point of each session and we synchronize the other signals according to this starting point. After the synchronization, we sample the signals with $f_s = 2$ Hz.

C. Cellular Neural Network

CNN was suggested by Chua and Yang [64]. They presented it as a universal neuro-system framework expressed by a system of differential equations that demonstrates the relationship between nonlinear units/cells. CNN combines the advantages of ordinary ANN and cellular automata (CA) in one platform. However, it differs from CA and ANN by its nonlinear dynamical representation of the interconnection between the adjacent cells. The generally proposed state equation of a CNN cell is given in

$$\frac{dx_i(t)}{dt} = -x_i(t) + \sum_{j=1}^{n} \boldsymbol{\omega}_{1_{i,j}} y_j(t) + \sum_{j=1}^{m} \boldsymbol{\omega}_{2_{i,j}} u_j(t) + \boldsymbol{\varepsilon}_i \quad (2)$$

$$y_i(t) = \frac{1}{2}(|x_i + 1| - |x_i - 1|) \quad (3)$$

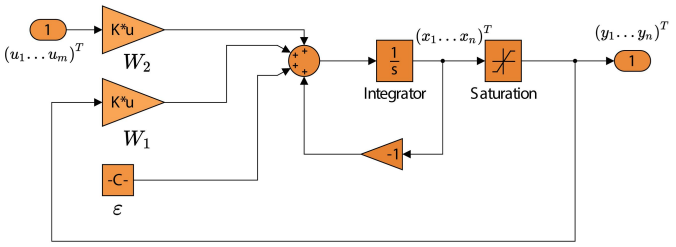

Fig. 8. Simulink CNN model (SimModel1).

where $x_i(t)$ and $y_i(t)$ represent the system state and the local output of the CNNs i_{th} cell, respectively, $u_i(t)$ is the i_{th} input, $\boldsymbol{W}_1 = (\boldsymbol{\omega}_{1_{1,1}} \dots \boldsymbol{\omega}_{1_{n,n}})$ is the CNN feedback template; $\boldsymbol{W}_2 = (\boldsymbol{\omega}_{2_{1,1}} \dots \boldsymbol{\omega}_{2_{n,m}})$ is the CNN control template, $\boldsymbol{\varepsilon}_i$ is a bias, and n and m are the number of cells and inputs, respectively. CNN is a system of differential equations, where (2) and (3) have to be solved in order to generate the related CNN output. This done using MATLAB Simulink [65]. In Fig. 8, the Simulink scheme of the CNN model is presented. Since the studied data are delivered from four types of sensors, representing different physical actions, we use a CNN model for each sensor type. Then, the local output of each CNN is connected to the final platform output through a linear regressor

$$\hat{g}(t) = \boldsymbol{W}^{\textbf{global}} \boldsymbol{Y}(t) \quad (4)$$

where $\boldsymbol{Y} = (y_1^{\textbf{eeg-cnn}} \dots y_n^{\textbf{eeg-cnn}}, y_1^{\textbf{ecg-cnn}} \dots y_n^{\textbf{ecg-cnn}}, y_1^{\textbf{eda-cnn}} \dots y_n^{\textbf{eda-cnn}}, and\, y_1^{\textbf{chds-cnn}} \dots y_n^{\textbf{chds-cnn}}, 1)$ is a vector of all four CNNs outputs. $\boldsymbol{W}^{\textbf{global}}$ is the output linear regression template. In Fig. 9, the related Simulink scheme of the multimodal driver state estimation is illustrated. All input signals are first mapped using principle components analysis (PCA) [66] to reduce the dimensionality of the inputs by selecting the most significant features. This is done with the MATLAB PRTools toolbox for pattern recognition [67]. The output of PCA mapping is then connected to four CNN blocks (one block for each sensor type). Each CNN block contains the same scheme (with different templates), as shown in Fig. 8. The CNN outputs are multiplexed and biased (linear regressor) with a constant to a single vector. The output of the multiplexer is either used to identify the linear regression template $W^{\textbf{global}}$ during the training phase (Y) or further processes according to (4), which gives the estimated driver state that is used for the operating/testing phase.

D. Learning Technique

The goal of training a CNN is the identification of the feedback templates, the control templates, and the biases and, hence, configures the CNN state equation. In this regard, many methods have been proposed. One group uses gradient-based methods such as the backpropagation proposed in [15]. Another group of methods follows evolutionary computation, where a genetic algorithm is most common to design CNN templates [16], [17]. Another more recent method is particle swarm optimization [68], [69]. The main challenge of the classical learning techniques is the time-consumption in which they may increase tremendously when dealing with the

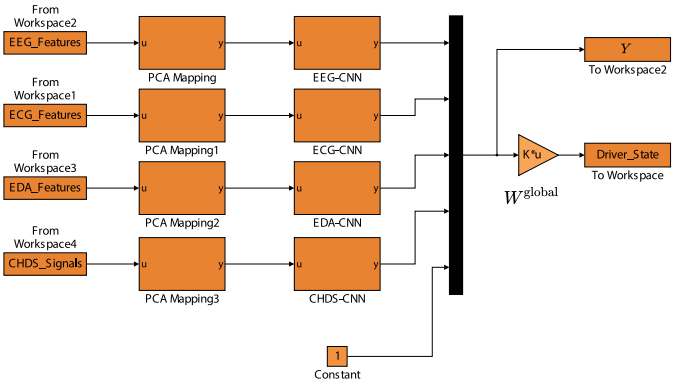

Fig. 9. CNN driver state estimation Simulink model (SimModel2).

highly dimensional CNN (i.e., with a large number of cells). To overcome this issue, we train CNN as an ESN. ESN is an innovative approach of training RNN that has presented excellent performance in the forecasting of either nonlinear or non-Gaussian dynamical sequences and classification. Originally, ESN was proposed by Jaeger back in the year 2001 [18]. In ESN, the state feedback templates, the control templates, and biases templates are randomly generated. The random generation approach when it is associated with a high number of neurons extract high level features from the inputs. The random generation process is done as follows.

1) $\boldsymbol{W}_1$ ($n \times n$ matrix) is generated as sparse matrix from $\mathcal{N}(0, 1)$ and a sparseness measure of 0.5. The resultant matrix is then divided by its own largest absolute eigenvalue. These generating constrains are important for the stability of the network as suggested in [70].
2) $\boldsymbol{W}_2$ ($n \times m$ matrix) and $\boldsymbol{\varepsilon}$ ($n \times 1$ vector) are generated randomly from $\mathcal{N}(0, 1)$ and scaled by a factor equal to 0.1.

After the four (EEG-CNN, ECG-CNN, EDA-CNN, and CHDS-CNN) CNN templates are generated, finally a global output linear regressor is trained using the ridge regression (RR) [70]

$$\boldsymbol{W}^{\mathbf{global}} = g(t)\boldsymbol{Y}(t)^T(\boldsymbol{Y}(t)\boldsymbol{Y}(t)^T + \beta \boldsymbol{I})^{-1} \tag{5}$$

where g(t) is the desired output, $\boldsymbol{I}$ is the identity matrix, and β is the regularization coefficient, which is determined using cross validation technique. It is necessary to add β in the RR to avoid an ill-conditioned problem of the regular least squares, which may occur if $\boldsymbol{Y}(t)\boldsymbol{Y}(t)^{\mathrm{T}}$ is singular or nearly singular.

E. Learning Algorithm for CNN

As it is explained in Section III-D, the model training is done using two steps: first an unsupervised step using the ESN approach and then a supervised step to identify the linear regressor template $W^{\mathbf{global}}$. By investigating the goal of the proposed model, which is estimating the driver state, we consider the following key points.

1) A comprehensive training (in-sample) data set that contains sensors data associated with a known driver state must be provided.

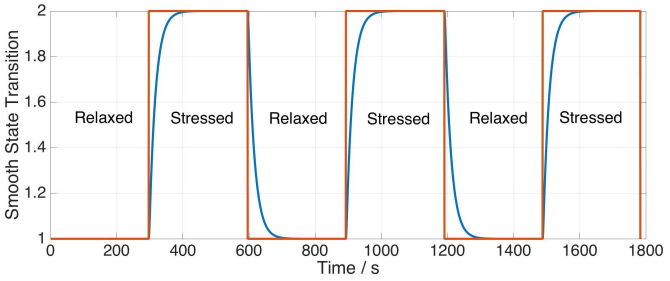

Fig. 10. Square driver state transition (red) versus the smooth driver state transition (blue).

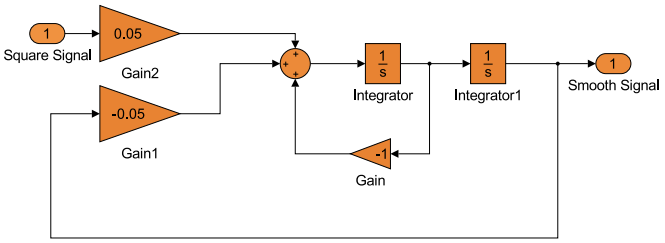

Fig. 11. Simulink driver state signal transformation (SimModel3).

TABLE I
SIMULINK CONFIGURATION PARAMETERS

Solver type	Fixed-step
Solver	ode1 (Euler)
Step size	0.5 with holding final value
Initial condition	CNN cells initial state is zero

2) The driver state is an accumulated state (transition between two states is not immediate and is subject to a transient phase). Considering this fact, Fig. 10 shows the used driver state smooth and sharp transition. The transformation between the sharp transition signal into the smooth one is done using the Simulink model in Fig. 11, which represents the second-order low-pass filter. In this paper, we consider a phase of 2 min (120 s) for transition and 3 min (240 s) for convergence at each state.
3) The synchronized sensor data (see Section III-B) are taken as input to the driver state estimation Simulink model.
4) Simulink is configured as indicated in Table I.
5) We use the following accuracy metric:

$$\text{Accuracy} = \frac{\text{Number of correctly classified samples}}{\text{Total number of test samples}}. \tag{6}$$

6) Following cross validation strategy, we divide the in-sample data set into ten sets (nine sets for learning and one set for validation).
7) The training process is done as described in Algorithm 1.

Algorithm 1 Driver Estimation System Learning Algorithm

Input: Synchronized sensor data,
Output: CNN templates, $W^{\mathbf{global}}$
Generate CNNs Templates following Echo state network rules in Sec. III-D
Set $W^{\mathbf{global}}$ to 0
for $n = 50, 100, 150, 1000, 2000$ **do**
for $\beta = 0.1, 0.01, 0.001, 0.0001, 0.00001$ **do**
for $i = 1, ..10$ **do**
Using the i^{th} learning dataset
Run SimModel2
Read Y from SimModel2
Using Y AND g (smooth driver state signal)
Estimate $W^{\mathbf{global}}$ using Eq. (5)
Using the i^{th} validation dataset and the estimated $W^{\mathbf{global}}$
Run SimModel2
Read Driver_State from SimModel2
Calculate the system accuracy using Eq. (6)
Set Accuracy to $Cross\_Validation\_Perf(i)$
end for
Set $System\_Parameters\_Perf(n, \beta)$ = average value of $Cross\_Validation\_Perf$
end for
end for
Select best CNNs system configuration that corresponds to the minimum $System\_Parameters\_Perf$

Algorithm 2 Driver Estimation System Operation Algorithm

Input: Synchronized sensor data,
Output: Driver State
Using the testing dataset (out-of-sample dataset)
Using trained CNN (from Algorithm 1)
Run SimModel2
Read Y from SimModel2
Read Driver_State from SimModel2
Calculate the system accuracy using Eq. (6)

F. Operation Algorithm for CNN

After the computation of CNN templates and $W^{\mathbf{global}}$, we use Algorithm 2 to evaluate our model on testing (out-of-sample) data set.

IV. Experimental Setup and Results

A. Capacitive Sensor Evaluation

Various setups are considered for the sensor evaluation. The steering wheel is equipped with two sensor mats (on the left and right sides) covered with a bend and stretchable synthetic material with an approximate thickness of $h_c = 1$ mm. This is done to demonstrate the functionality of the sensor mats even when they are mounted below the surface of the steering wheel rim [see Fig. 12(a)]. In the first setup (A), the driver grasps and releases the steering wheel three times without moving it. In the second setup (B), the steering wheel is used in combination with a driving simulator platform [see Fig. 1], where the driver is placed in a virtual traffic environment. A snapshot of the online visualization of the hand position for demonstration purposes is shown in Fig. 12(b). The area, where a hand can be detected is subdivided into the 12 regions A1–A12. These regions are directly related to the transmitter electrodes Tx1–Tx12 of both sensor mats. The detection threshold value is set to $\Delta C_{\text{th}} = 1.66$ pF. The threshold value 2Δ for the energy efficient data transmission is set to 0.06 pF.

1) Setup A: In Fig. 13, the results for a human grasping the steering wheel three times at different areas are presented. After touching the surface of the steering wheel, the coupling effect prevails and ΔC increases immediately at time $t = 18.5$ s at transmitter Tx5–Tx8 detecting a touch at areas A5–A8. While grasping, the measurement signals stay stable and drop to zero when the steering wheel is released at $t = 20.5$ s. The detection results clearly show the grasping positions at area A5 and A6 and A7 and A8 for the right and left hands, respectively. After each release, all sensor signals stay stable around zero. During the second grasp, the hands are detected at areas A3 and A4 and A9 and A10. Finally, the steering wheel is grasped during the time interval $t = 25$–27 s at areas A1 and A2 and A11 and A12.

2) Setup B: Fig. 14 shows the results when a driver grasps the steering wheel, moves it to the left and right sides, and releases it three times at different areas A1–A12. In comparison with the results in Fig. 13, the sensor signals are not as stable as in the static case due to the slight movement of the hands on the steering wheel while steering to the left and right sides. In addition, during the second grasp, the left and right thumbs are slightly lifted around $t = 19$ s and $t = 21$ s, where the sensor signals Tx9 and Tx3 drop slightly, respectively. Moreover, it can be seen that the left hand of the driver partially touches area A8 and A2 as well.

In Fig. 15, the results while a test person is driving on a track in a virtual traffic environment are presented. The sensor signals stay stable even if the driver is steering heavily and the hand position can be clearly detected throughout the entire driving simulation. The driver removes his left hand between $t = 237$–245 s completely from the rim followed by a smooth steering with both hands till $t = 275$ s. Afterward, the driver starts to steer heavily again and his hands are sliding around on the steering wheel.

The experimental results of both setups demonstrate the sensor's capabilities to reliably detect the position of the hands on a steering wheel. In Section (IV-B), the sensor is used as an input for a driver state detection system for further analysis.

B. Driver State Estimation Study

The experimental setup to collect the data for the driver state system to estimate the stress level is defined as follows: each participant has to drive in two different scenarios. In Scenario I, the participants are driving for 5 min in a virtual traffic environment without any restrictions. In scenario II, the participants are driving in the same environment for 5 min but shall keep the vehicle within a certain speed limit $v = 60$–100 km/h and answer questions, simultaneously. Each time the driver is not answering the question properly or does not stay within

(a) (b)

Fig. 12. (a) Steering wheel fully equipped with two sensor mats. The orange and brown strips show the position of the sensor mats on the left and right sides, respectively. (b) Visualization of the hand position detection. The green LEDs show the covered area (A1–A12), where a human hand, touching the rim of the steering wheel, can be detected.

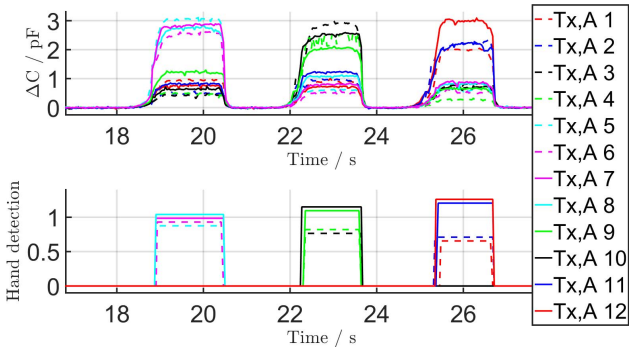

Fig. 13. Raw sensor signals and detection results when two hands grasping the steering wheel rim three times. The sensor mats are covered by a synthetic material. It should be noted that the detection results are shown at different levels for each area for visualization purposes only.

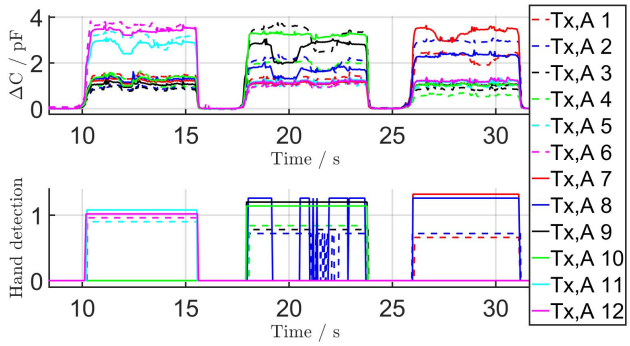

Fig. 14. Raw sensor signals and detection results for two hands grasping the steering wheel rim and move it 90° to the left and right sides, three times. The sensor mats are covered by a synthetic material. It should be noted that the detection results are shown at different levels for each area for visualization purposes only.

the defined speed limit, and two different acoustics signal as feedback are given. The two scenarios are considered to represent two driver states, which are nondistracted/relaxed and distracted/stressed. These two states are the targets of our study. A total of 22 drivers with previous driving experience and no health problems participated in this paper.

As it is mentioned in Section III-C, the main challenge of the related work is subject dependence. This challenge is mainly considered in our evaluation by testing the performance on unexperienced/untrained subjects (participants). Therefore, the evaluation is done using "threefold" cross validation over the 22 participants. For each step of the three validations, the data of 15 participants are used to train the model (in-sample data set). Then, the test is done on data of the remaining seven participants (out-of-sample data set). In this case, the evaluation treats the subject-independent case, since the test participants data for the two studied scenarios are not considered in the training. For each scenario, the first 2 min are considered as a transient phase and not included in the training or testing process. This transient phase represents the supposed time delay until the driver gets into the nondistracted/relaxed or the distracted/stressed phase. Considering the sampling rate $f_s = 2$ Hz, the three remaining minutes in each scenario give 360 ($3 \times 60 \times 2$) data samples to be used. For two scenarios per participant and 22 participants, this results in 15 840 samples. At each cross validation step, data are split into 10 800 training and 5840 testing samples. Each sample is a vector of 623 features, combining data from all sensors. Before applying the feature vector to the system, we reduce the dimensionality using PCA. The PCA is applied on each sensor signal individual with a fraction of cumulative variance equal to $\sigma_c = 0.9$, which represents how significant the selected features are.

To benchmark our CNN model, we select the following four well known classification concepts: 1) SVM with radial basis function SVM with radial basis function (RBSVM) [5], [6]; 2) naive Bayes classifier [71]; 3) decision tree classifier [72]; and 4) ANN [73]. We use Weka data mining software [74] to train and test the selected classifiers with the configuration parameters given in Table II. Furthermore, it includes the CNN configuration parameters obtained using Algorithm 1.

The evaluation is addressed based on different combinations of sensors. The related results are presented in Table III. The accuracy of all considered classifiers is calculated using 6. We summarize the results as follows.

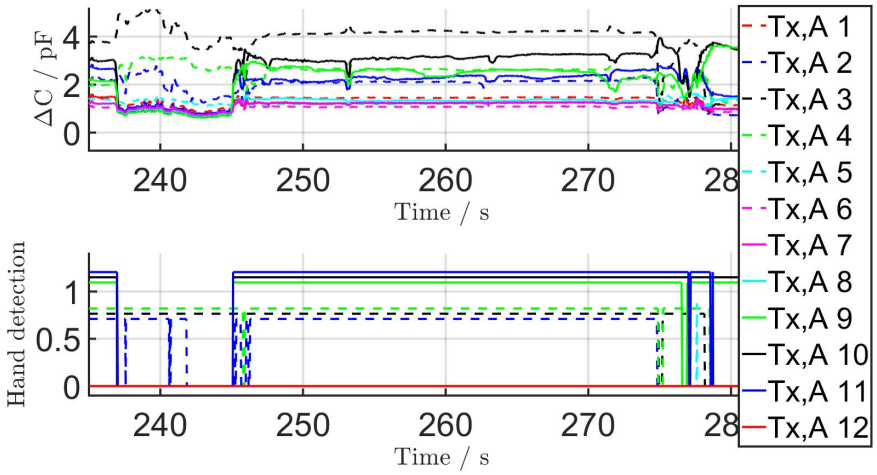

Fig. 15. Sensor signals and detection results for a human driving around in a virtual traffic environment. The sensor mats are covered by a synthetic material. It should be noted that the detection results are shown at different levels for each area for visualization purposes only.

TABLE II
USED CLASSIFIERS CONFIGURATION PARAMETERS

Classifier	Framework	Type	Parameters
RBSVM	Weka	C-SVC	KernelType= radial basis function, eps= 0.001, gamma= 0.0001
NB	Weka	NaiveBayes -k	UseKernelEstimator= True
DT	Weka	RandomForest	default
ANN	Weka	Multilayer Perceptron	hiddenlayer=20, learningRate=0.1, momentum=0.2
CNN	Matlab Simulink	Echo State	$n = 150$, $\beta = 0.0001$

TABLE III
DETECTION ACCURACY WITH RESPECT TO THE SENSORS DATA COMBINATION

		Accuracy (Physiological sensors alone) %					Accuracy with CHDS (Physiological sensors combined with CHDS) %				
	Physiological Sensor	CNN	RBSVM	NB	DT	ANN	CNN	RBSVM	NB	DT	ANN
Single sensor	ECG	35	**48**	45	32	34	**64**	62	60	60	59
	EDA	**72**	67	58	65	63	**75**	71	59	69	70
	EEG	**65**	62	59	64	60	**76**	73	69	70	69
Multiple sensors	EDA + ECG	**62**	55	59	61	54	**85**	72	68	80	74
	EEG + ECG	68	**70**	63	66	63	**86**	77	74	76	72
	EEG + EDA	**79**	74	75	77	70	**88**	78	80	84	76
	EEG + EDA + ECG	**82**	76	70	74	72	**92**	82	77	84	76

1) The detection accuracy using all available sensors is 92%, which is a very promising result if we consider that the evaluation is based on a subject-independent case.
2) The CHDS increases the performance significantly by 10% when it is combined with multiple physiological sensors. A small improvement is observed even if CHDS is combined with only a single physiological sensor. The advantage of the CHDS is its ability to remove the negative effect of subject dependence.
3) Overall, for this case study, our proposed CNN classifier outperforms all the other benchmarking classifiers.
4) ECG cannot be used in this setup as a single sensor and needs to be combined with EEG, EDA, or CHDS sensors.
5) EEG yields the most information with respect to stress detection, since it improves the results significantly when it is combined with other sensors.

V. CONCLUSION

We present a CNN-based driver state detection system to monitor the stress level of a driver. It combines the input of both the state-of-the-art physiological sensors and a novel capacitive touch and position detection sensor. First, the CHDS for steering wheels with wireless and energy efficient data transmissions is presented and evaluated. Second, the proposed driver state detection system is evaluated by conducting a study with 22 participants on a driving simulator platform. The classification results of the CNN (benchmarked with other state-of-the-art machine learning methods) show a significant improvement of the accuracy, whenever the physiological sensor(s) are combined with information of the CHDS. In case of taking all available sensor inputs into account, the CHDS improves the accuracy by 10%. In addition, the CHDS is ready for easy retrofit of any car due to the wireless data transmission for further applications, e.g., conducting further studies in a real traffic environment on the road. A considerable aspect for the future is the measurement of the physiological signals with a sensor embedded in the driver seat, which is more convenient for the driver.

REFERENCES

[1] National Highway Traffic Safety Administration, "Distracted driving 2009," U.S. Dept. Transp., Washington DC, USA, Tech. Rep., 2010.
[2] S. Lüke, O. Fochler, T. Schaller, and U. Regensburger, "Stauassistenz und—Automation," in *Handbuch Fahrerassistenzsysteme*. Fachmedien Wiesbaden, Germany: Springer, 2015, pp. 995–1007.
[3] J. F. Coughlin, B. Reimer, and B. Mehler, "Monitoring, managing, and motivating driver safety and well-being," *IEEE Pervasive Comput.*, vol. 10, no. 3, pp. 14–21, Jul. 2011.
[4] S. Mühlbacher-Karrer, L.-M. Faller, R. Hamid, and H. Zangl, "A wireless steering wheel gripping sensor for hands on/off detection," in *Proc. IEEE Sensors Appl. Symp. (SAS)*, Apr. 2016, pp. 1–5.
[5] A. Marconato, M. Hu, A. Boni, and D. Petri, "Dynamic compensation of nonlinear sensors by a learning-from-examples approach," *IEEE Trans. Instrum. Meas.*, vol. 57, no. 8, pp. 1689–1694, Sep. 2008.
[6] K. Ganesan, U. R. Acharya, C. K. Chua, C. M. Lim, and K. T. Abraham, "One-class classification of mammograms using trace transform functionals," *IEEE Trans. Instrum. Meas.*, vol. 63, no. 2, pp. 304–311, Feb. 2014.

[7] S. Foucher, M. Germain, J. M. Boucher, and G. B. Benie, "Multisource classification using ICM and Dempster–Shafer theory," *IEEE Trans. Instrum. Meas.*, vol. 51, no. 2, pp. 277–281, Apr. 2002.

[8] D. Lo, R. A. Goubran, and R. M. Dansereau, "Robust joint audio-video talker localization in video conferencing using reliability information—II: Bayesian network fusion," *IEEE Trans. Instrum. Meas.*, vol. 54, no. 4, pp. 1541–1547, Apr. 2005.

[9] W. Li, A. Monti, and F. Ponci, "Fault detection and classification in medium voltage DC shipboard power systems with wavelets and artificial neural networks," *IEEE Trans. Instrum. Meas.*, vol. 63, no. 11, pp. 2651–2665, Nov. 2014.

[10] H. Marzi, "Modular neural network architecture for precise condition monitoring," *IEEE Trans. Instrum. Meas.*, vol. 57, no. 4, pp. 805–812, Apr. 2008.

[11] X. Li and A. G.-O. Yeh, "Neural-network-based cellular automata for simulating multiple land use changes using GIS," *Int. J. Geograph. Inf. Sci.*, vol. 16, no. 4, pp. 323–343, Apr. 2002.

[12] H. Li, X. Liao, C. Li, H. Huang, and C. Li, "Edge detection of noisy images based on cellular neural networks," *Commun. Nonlinear Sci. Numer. Simul.*, vol. 16, no. 9, pp. 3746–3759, Oct. 2011.

[13] R. Perfetti, E. Ricci, D. Casali, and G. Costantini, "Cellular neural networks with virtual template expansion for retinal vessel segmentation," *IEEE Trans. Circuits Syst. II, Express Briefs*, vol. 54, no. 2, pp. 141–145, Feb. 2007.

[14] M. Milanova and U. Büker, "Object recognition in image sequences with cellular neural networks," *Neurocomputing*, vol. 31, no. 1, pp. 125–141, 2000.

[15] B. Mirzai, Z. Cheng, and G. S. Moschytz, "Learning algorithms for cellular neural networks," in *Proc. IEEE Int. Symp. Circuits Syst.*, Jun. 1998, pp. 159–162.

[16] A. Fasih, J. C. Chedjou, and K. Kyamakya, "Cellular neural network trainer and template optimization for advanced robot locomotion, based on genetic algorithm," in *Proc. 15th Int. Conf. Mechatronics Mach. Vis. Practice (M2VIP)*, Dec. 2008, pp. 317–322.

[17] S. SanthoshKumar, J. Vignesh, L. R. Rangarajan, V. S. Narayanan, K. M. Rangarajan, and A. L. Venkatkrishna, "A fast time scale genetic algorithm based image segmentation using cellular neural networks (CNN)," in *Proc. IEEE Int. Conf. Signal Process. Commun. (ICSPC)*, Nov. 2007, pp. 908–911.

[18] H. Jaeger, "The echo state approach to analysing and training recurrent neural networks-with an erratum note," German Nat. Res. Center Inf. Technol., Bonn, Germany, GMD Tech. Rep., 2001, vol. 148, p. 34,

[19] H. Jaeger, "Long short-term memory in echo state networks: Details of a simulation study," Jacobs Univ. Bremen, Bremen, Germany, Tech. Rep. 27, 2012.

[20] T. Roska and L. O. Chua, "The CNN universal machine: An analogic array computer," *IEEE Trans. Circuits Syst. II, Analog Digit. Signal Process.*, vol. 40, no. 3, pp. 163–173, Mar. 1993.

[21] P. Kinget and M. S. J. Steyaert, "A programmable analog cellular neural network CMOS chip for high speed image processing," *IEEE J. Solid-State Circuits*, vol. 30, no. 3, pp. 235–243, Mar. 1995.

[22] Z. Nagy and P. Szolgay, "Configurable multilayer CNN-UM emulator on FPGA," *IEEE Trans. Circuits Syst. I, Fundam. Theory Appl.*, vol. 50, no. 6, pp. 774–778, Jun. 2003.

[23] T.-Y. Ho, P.-M. Lam, and C.-S. Leung, "Parallelization of cellular neural networks on GPU," *Pattern Recognit.*, vol. 41, no. 8, pp. 2684–2692, 2008.

[24] M. Tang, "Edge detection and image segmentation based on cellular neural network," in *Proc. Int. Conf. Bioinform. Biomed. Eng. (ICBBE)*, Jun. 2009, pp. 1–4.

[25] G. Brasseur, "Design rules for robust capacitive sensors," *IEEE Trans. Instrum. Meas.*, vol. 52, no. 4, pp. 1261–1265, Aug. 2003.

[26] B. George, H. Zangl, T. Bretterklieber, and G. Brasseur, "A novel seat occupancy detection system based on capacitive sensing," in *Proc. IEEE Instrum. Meas. Technol. Conf.*, Apr. 2008, pp. 1515–1519.

[27] *Smart Trunk Opener—STO, Datasheet, IEE a Sense for Inovation*, IEE Sense Innovation, Contern, Luxembourg, 2013.

[28] *Hands off Detection—HOD, Datasheet, IEE a Sense for Inovation*, IEE Sense Innovation, Contern, Luxembourg, 2015.

[29] T. Evarts, P. Balcom, J. Evarts, E. Balcom, K. Balcom, and B. Evarts, "Steering wheel hand position sensing device," U.S. Patent 8 564 424, Oct. 22, 2013.

[30] D. Güzelocak, S. Shokr, and S. Zaidan, "Monitoring and emergency system for motor vehicles," U.S. Patent EP20 110 793 650, Jul. 10, 2013.

[31] I. M. D. Silva, L. A. Guedes, and F. Vasques, "Performance evaluation of a compression algorithm for wireless sensor networks in monitoring applications," in *Proc. IEEE Int. Conf. Emerg. Technol. Factory Autom. (ETFA)*, Sep. 2008, pp. 672–678.

[32] K. Kaija, V. Pekkanen, M. Mäntysalo, and P. Mansikkamäki, "Applicability of inkjet technology for electronics manufacturing," in *Proc. SMTA Int. Conf.*, 2008, pp. 1–7.

[33] B. Andò and S. Baglio, "Inkjet-printed sensors: A useful approach for low cost, rapid prototyping [instrumentation notes]," *IEEE Instrum. Meas. Mag.*, vol. 14, no. 5, pp. 36–40, Oct. 2011.

[34] M. F. Farooqui, C. Claudel, and A. Shamim, "An inkjet-printed buoyant 3-D Lagrangian sensor for real-time flood monitoring," *IEEE Trans. Antennas Propag.*, vol. 62, no. 6, pp. 3354–3359, Jun. 2014.

[35] S. Cruz, D. Dias, J. C. Viana, and L. A. Rocha, "Inkjet printed pressure sensing platform for postural imbalance monitoring," *IEEE Trans. Instrum. Meas.*, vol. 64, no. 10, pp. 2813–2820, Oct. 2015.

[36] S. Kim, Y. Kawahara, A. Georgiadis, A. Collado, and M. M. Tentzeris, "Low-cost inkjet-printed fully passive RFID tags for calibration-free capacitive/haptic sensor applications," *IEEE Sensors J.*, vol. 15, no. 6, pp. 3135–3145, Jun. 2015.

[37] J. Virtanen, L. Ukkonen, T. Björninen, A. Z. Elsherbeni, and L. Sydanheimo, "Inkjet-printed humidity sensor for passive UHF RFID systems," *IEEE Trans. Instrum. Meas.*, vol. 60, no. 8, pp. 2768–2777, Aug. 2011.

[38] N. Jeranče, D. Vasiljević, N. Samardžić, and G. Stojanović, "A compact inductive position sensor made by inkjet printing technology on a flexible substrate," *Sensors*, vol. 12, no. 2, pp. 1288–1298, 2012.

[39] J. A. Healey and R. W. Picard, "Detecting stress during real-world driving tasks using physiological sensors," *IEEE Trans. Intell. Transp. Syst.*, vol. 6, no. 2, pp. 156–166, Jun. 2005.

[40] J. Kim and E. André, "Emotion recognition based on physiological changes in music listening," *IEEE Trans. Pattern Anal. Mach. Intell.*, vol. 30, no. 12, pp. 2067–2083, Dec. 2008.

[41] D. Bian, J. Wade, A. Swanson, Z. Warren, and N. Sarkar, "Physiology-based affect recognition during driving in virtual environment for autism intervention," in *Proc. 2nd Int. Conf. Physiol. Comput. Syst.*, 2015, pp. 1–9.

[42] Y. Liang, M. L. Reyes, and J. D. Lee, "Real-time detection of driver cognitive distraction using support vector machines," *IEEE Trans. Intell. Transp. Syst.*, vol. 8, no. 2, pp. 340–350, Jun. 2007.

[43] Y. Liang and J. D. Lee, "A hybrid Bayesian Network approach to detect driver cognitive distraction," *Transp. Res. C, Emerg. Technol.*, vol. 38, pp. 146–155, Jan. 2014.

[44] Y. Liang and J. D. Lee, "Combining cognitive and visual distraction: Less than the sum of its parts," *Accident Anal. Prevention*, vol. 42, no. 3, pp. 881–890, May 2010.

[45] M. Miyaji, H. Kawanaka, and K. Oguri, "Driver's cognitive distraction detection using physiological features by the AdaBoost," in *Proc. 12th Int. IEEE Conf. Intell. Transp. Syst.*, Oct. 2009, pp. 1–6.

[46] Y. Dong, Z. Hu, K. Uchimura, and N. Murayama, "Driver inattention monitoring system for intelligent vehicles: A review," *IEEE Trans. Intell. Transp. Syst.*, vol. 12, no. 2, pp. 596–614, Jun. 2011.

[47] T. Schlegl, T. Kröger, A. Gaschler, O. Khatib, and H. Zangl, "Virtual whiskers—Highly responsive robot collision avoidance," in *Proc. IEEE/RSJ Int. Conf. Intell. Robots Syst. (IROS)*, Nov. 2013, pp. 5373–5379.

[48] S. Mühlbacher-Karrer, L.-M. Faller, H. Zangl, T. Schlegl, and M. Moser, "Short range capacitive proximity sensing," in *Proc. 2nd Workshop Alternative Sens. Robot Perception Beyond Laser Vis.*, Hamburg, Germany, Oct. 2015, pp. 1–3.

[49] *nRF51822—Product Specification*, Nordic Semicond., Trondheim, Norway, 2014.

[50] *CapTouch Programmable Controller for Single-Electrode Capacitance Sensors AD7147, Datasheet*, Analog Devices, Cambridge, MA, USA, 2015.

[51] H. Zangl, M. Zine-Zine, and S. Mühlbacher-Karrer, "TEDS extensions toward energy management of wireless transducers," *IEEE Sensors J.*, vol. 15, no. 5, pp. 2587–2594, May 2015.

[52] Empatica. *Empatica E4 Wristband—EDA Sensor*, accessed on Aug. 6, 2016. [Online]. Available: https://www.empatica.com/e4-wristband

[53] Great Lakes Neurotechnologies. *BioRadio—ECG Sensor*, accessed on Aug. 6, 2016. [Online]. Available: https://glneurotech.com/bioradio/

[54] EMOTIV. *Emotiv Epoc+—EEG Sensor*, accessed on Aug. 6, 2016. [Online]. Available: http://emotiv.com/epoc/

[55] R. W. Homan, J. Herman, and P. Purdy, "Cerebral location of international 10–20 system electrode placement," *Electroencephalogr. Clin. Neurophysiol.*, vol. 66, no. 4, pp. 376–382, 1987.

[56] T. Wartzek, B. Eilebrecht, J. Lem, H.-J. Lindner, S. Leonhardt, and M. Walter, "ECG on the road: Robust and unobtrusive estimation of heart rate," *IEEE Trans. Biomed. Eng.*, vol. 58, no. 11, pp. 3112–3120, Nov. 2011.
[57] M. Benedek and C. Kaernbach, "Decomposition of skin conductance data by means of nonnegative deconvolution," *Psychophysiology*, vol. 47, no. 4, pp. 647–658, Jul. 2010.
[58] M. P. Tarvainen, J.-P. Niskanen, J. A. Lipponen, P. O. Ranta-Aho, and P. A. Karjalainen, "Kubios HRV—Heart rate variability analysis software," *Comput. Methods Programs Biomed.*, vol. 113, no. 1, pp. 210–220, Jan. 2014.
[59] A. Subasi, "EEG signal classification using wavelet feature extraction and a mixture of expert model," *Expert Syst. Appl.*, vol. 32, no. 4, pp. 1084–1093, May 2007.
[60] U. Orhan, M. Hekim, and M. Ozer, "EEG signals classification using the K-means clustering and a multilayer perceptron neural network model," *Expert Syst. Appl.*, vol. 38, no. 10, pp. 13475–13481, Sep. 2011.
[61] A. Konar and A. Chakraborty, *Emotion Recognition: A Pattern Analysis Approach*. Hoboken, NJ, USA: Wiley, 2014.
[62] P. C. Petrantonakis and L. J. Hadjileontiadis, "Emotion recognition from EEG using higher order crossings," *IEEE Trans. Inf. Technol. Biomed.*, vol. 14, no. 2, pp. 186–197, Mar. 2010.
[63] K. Takahashi, "Remarks on emotion recognition from bio-potential signals," in *Proc. Int. Conf. Auto. Robots Agents*, 2005, pp. 1–6.
[64] L. O. Chua and L. Yang, "Cellular neural networks: Applications," *IEEE Trans. Circuits Syst.*, vol. 35, no. 10, pp. 1273–1290, Oct. 1988.
[65] *MATLAB, Version 7.14.0 (R2013b)*, MathWorks Inc., Natick, MA, USA, 2013.
[66] K. Fukunaga, *Introduction to Statistical Pattern Recognition*. San Francisco, CA, USA: Academic, 2013.
[67] F. van der Heijden, R. Duin, D. de Ridder, and D. M. J. Tax, *Classification, Parameter Estimation and State Estimation: An Engineering Approach Using MATLAB*. Hoboken, NJ, USA: Wiley, 2005.
[68] H.-L. Wei and S. A. Billings, "Generalized cellular neural networks (GCNNs) constructed using particle swarm optimization for spatio-temporal evolutionary pattern identification," *Int. J. Bifurcation Chaos*, vol. 18, no. 12, pp. 3611–3624, 2008.
[69] T.-J. Su, J.-C. Cheng, and Y.-D. Sun, "Particle swarm optimization with time-varying acceleration coefficients based on cellular neural network for color image noise cancellation," in *Proc. 6th Int. Conf. Digit. Telecommun. (ICDT)*, 2011, pp. 109–115.
[70] M. Lukoševičius, "A practical guide to applying echo state networks," in *Neural Networks: Tricks of the Trade*. Berlin, Germany: Springer, 2012, pp. 659–686.
[71] S. Srivastava, M. R. Gupta, and B. A. Frigyik, "Bayesian quadratic discriminant analysis," *J. Mach. Learn. Res.*, vol. 8, no. 6, pp. 1277–1305, Jun. 2007.
[72] T. K. Ho, "The random subspace method for constructing decision forests," *IEEE Trans. Pattern Anal. Mach. Intell.*, vol. 20, no. 8, pp. 832–844, Aug. 1998.
[73] W. Yan, "Toward automatic time-series forecasting using neural networks," *IEEE Trans. Neural Netw. Learn. Syst.*, vol. 23, no. 7, pp. 1028–1039, Jul. 2012.
[74] M. Hall, E. Frank, G. Holmes, B. Pfahringer, P. Reutemann, and I. H. Witten, "The WEKA data mining software: An update," *ACM SIGKDD Explorations Newslett.*, vol. 11, no. 1, pp. 10–18, Nov. 2009.

Stephan Mühlbacher-Karrer received the Dipl.Ing. degree in telematics from the Graz University of Technology, Graz, Austria, in 2012, where he focused on autonomous robots and telecommunications. He is currently pursuing the Ph.D. degree with Alpen-Adria-Universität Klagenfurt, Klagenfurt, Austria, focusing on capacitive sensing for robotic applications.

From 2012 to 2013, he was with Gigatronik Ingolstadt GmbH, Gaimersheim, Germany, working for Audi Electronics Venture GmbH, Gaimersheim, where he was involved in the pre-development for piloted driving. He is currently a Research and Teaching Assistant with the Sensors and Actuators Group, Institute of Smart System-Technologies, Alpen-Adria-Universität Klagenfurt. His current research interests include near field sensor technology, signal processing, and autonomous robots.

Ahmad Haj Mosa received the B.S. degree in mechatronics engineering from Tishreen University, Lattakia, Syria, in 2008, the M.Sc. degree in health care IT from the Carinthia University of Applied Science, Klagenfurt, Austria, and the Ph.D. degree from Alpen-Adria-Universität Klagenfurt, Klagenfurt, in 2016.

He is currently a University Assistant with the Institute of Smart System Technologies, Alpen-Adria-Universität Klagenfurt. He developed a variety of methods in the scope of human-machine interaction and machine learning. He has participated in several projects in the field of transportation informatics. His current research interests include machine vision, machine learning, applied mathematics, and neurocomputing.

Lisa-Marie Faller received the B.Sc. degree in systems engineering and the M.Sc. degree in systems design from the Carinthia University of Applied Sciences (CUAS), Villach, Austria, in 2011 and 2014, respectively. She is currently pursuing the Ph.D. degree with Alpen-Adria-Universität Klagenfurt, Klagenfurt, Austria. Her master thesis was titled Advanced Process Control of an Electrochemical Deposition Process for Semiconductor Fabrication.

She was with the Integrated Systems and Circuits Research Group, CUAS, focused on the design of color sensors fabricated in CMOS technology. In 2014, she joined the Sensors and Actuators Group, Alpen-Adria-Universität Klagenfurt, focused on robust design and statistical signal processing, where she was a Research and Teaching Assistant. Her current research interests include inkjet-printed capacitive sensing system for a MEMS micro-mirror as part of an infrared-spectrometer.

Mouhannad Ali received the B.Sc. degree in information technology from Syrian Virtual University, Damascus, Syria, in 2008, and the Diploma degree in health care IT from the Carinthia University of Applied Sciences, Klagenfurt, Austria. He is currently pursuing the Ph.D. degree with the Institute of Smart System Technologies, Alpen-Adria-Universität Klagenfurt, Klagenfurt.

His current research interests include signal processing, machine learning, and data mining.

Raiyan Hamid received the bachelor's degree in mechatronics engineering from Nelson Mandela Metropolitan University, Port Elizabeth, South Africa, and the M.Sc. degree from the Carinthia University of Applied Sciences, Villach, Austria, in 2015.

He served as a Project Assistant with the Sensors and Actuators Group, Alpen-Adria-Universität Klagenfurt, Klagenfurt, Austria, where he focused on smart transducers, wireless communication, and the Internet of Things and he took part in several European funded projects.

Mr. Hamid has been a member of the MEMS Microphones Verification Team, Infineon Technologies, Villach.

Hubert Zangl received the Dipl.Ing. degree in telematics, the Dr. Tech. degree in electrical engineering, and the Venia Docendi degree in sensors and instrumentation from the Graz University of Technology (TUG), Graz, Austria, in 2001, 2005, and 2009, respectively.

From 2010 to 2013, he was an Associate Professor of Sensors and Instrumentation with the Institute of Electrical Measurement and Measurement Signal Processing, TUG. Since 2013, he has been a Professor chairing Sensors and Actuators with the Institute of Smart System Technologies, Alpen-Adria-Universität Klagenfurt, Klagenfurt, Austria. He has authored or co-authored over 100 international scientific publications and holds several patents. His current research interests include the design and optimization of smart sensors and actuators, robustness, and reliability of sensors and actuators, sensor signal processing, autarkic wireless sensors, and energy harvesting.

Kyandoghere Kyamakya received the Ingenieur Civil degree in electrical engineering from the University of Kinshasa, Kinshasa, Congo, in 1990, and the Ph.D. degree in electrical engineering from the University of Hagen, Hagen, Germany, in 1999.

He was a Post-Doctoral Researcher of Mobility Management in Wireless Networks with the Leibniz University of Hannover, Hannover, Germany, where he was a Junior Professor of Positioning and Location Based Services, from 2002 to 2005. Since 2005, he has been a Full Professor of Transportation Informatics with Alpen-Adria-Universität Klagenfurt, Klagenfurt, Austria. His current research interests include modeling, simulation, and test-bed evaluations for the series of concepts in the frame of the application of information and communication technology in transportation, such as intelligent transportation systems, intelligent vehicles and mobile robotics systems, and intelligent logistics and supply chains.